atmosphere

MDPI

Article

Investigating the Role of the Low-Level Jet in Two Winters Severe Dust Rising in Southwest Iran

Rahman Parno [1], Amir-Hussain Meshkatee [1], Elham Mobarak Hassan [2], Nasim Hossein Hamzeh [3,*], Maggie Chel Gee Ooi [4] and Maral Habibi [5,*]

[1] Islamic Azad University Tehran Science and Research Branch, Tehran 14778-93855, Iran; rparno1354@gmail.com (R.P.); ameshkatee@srbiau.ac.ir (A.-H.M.)
[2] Department of Environment, Ahvaz Branch, Islamic Azad University, Ahvaz 61349-37333, Iran; emobarak.h@gmail.com
[3] Department Meteorology, Air and Climate Technology Company (ACTC), Tehran 15996-16313, Iran
[4] Centre of Tropical Climate Change System, Institute of Climate Change, University Kebangsaan Malaysia, Bangi 43600, Malaysia
[5] Department of Geography and Regional Science, University of Graz, 8010 Graz, Austria
* Correspondence: nasim.hosseinhamzeh@gmail.com (N.H.H.); maral.habibi@uni-graz.at (M.H.)

Abstract: The dust storms with local and non-local dust sources mostly affect Khuzestan province in southwest (SW) Iran. In this study, the role of the low-level jet in the activation of the internal dust events in SW Iran during two severe dust cases was investigated. For this purpose, the fifth-generation ECMWF reanalysis for the global climate and weather (ERA5) data was used to identify the synoptic patterns and the low-level jet (LLJ) characteristics in the study area. Furthermore, the images of the moderate resolution imaging spectroradiometer (MODIS) sensor, the outputs of the hybrid single-particle Lagrangian integrated trajectory (HYSPLIT) model, and a weather research and forecasting model coupled with chemistry (WRF-Chem) were used to investigate the propagation and transport of the dust particles. The results of the synoptic analysis in both dust cases show the simultaneous occurrence of the divergence zone associated with cyclonic curvature in the subtropical jet stream (STJ) at 300 hPa, causing convergence at 925 hPa, upward motion, and the development of low surface pressure in SW Iran. Examining the vertical wind profile shows the existence of the maximum horizontal wind speeds of 975 to 875 hPa, along with the positive and negative shear below and above it, respectively, which emphasizes the existence of the LLJ and its role in local dust emission. The results of the comparison between the satellite images, WRF-Chem, and HYSPLIT model outputs show the formation and transportation of dust particles from the inner regions of Khuzestan in SW Iran. The horizontal dust surface distribution, vertical raised dust mass, and kinetic energy transfers are well simulated by the WRF-Chem model when LLJ broke at 09:00 to 12:00 UTC. The most important finding of this research is that, for the first time, the role of low-level jet is investigated in the activation of internal dust events in SW Iran.

Keywords: dust events; low-level jet; WRF-Chem model; southwest Iran; HYSPLIT model

check for updates

Citation: Parno, R.; Meshkatee, A.-H.; Mobarak Hassan, E.; Hamzeh, N.H.; Chel Gee Ooi, M.; Habibi, M. Investigating the Role of the Low-Level Jet in Two Winters Severe Dust Rising in Southwest Iran. *Atmosphere* **2024**, *15*, 400. https://doi.org/10.3390/atmos15040400

Academic Editor: Avelino Eduardo Saez

Received: 2 January 2024
Revised: 11 March 2024
Accepted: 19 March 2024
Published: 25 March 2024

Copyright: © 2024 by the authors. Licensee MDPI, Basel, Switzerland. This article is an open access article distributed under the terms and conditions of the Creative Commons Attribution (CC BY) license (https://creativecommons.org/licenses/by/4.0/).

1. Introduction

The dust storm is a natural disaster, such as earthquakes, volcanoes, floods, drought, and storms, causing damage to urban environments and various infrastructures. This phenomenon occurs in many places globally, but it is far more common in arid and semi-arid areas than in the other regions throughout the world [1–3]. As a country in the Middle East, Iran is located in arid and semi-arid regions and suffers from disasters more frequently [4,5]. This phenomenon mainly affects southwest (SW) and west Iran, southeast (SE) Iran, and northern borders of the Persian Gulf [6–12]. West and SW Iran are mainly influenced by dust storms originated from deserts in Syria, Iraq, Saudi Arabia, and Kuwait [6–8,13,14]. More than 90 percent of dust particles originate from external sources,

whereas the contribution of internal dust sources is less than 8 percent in this area [15]. Also, Ahvaz (in SW Iran) is one of the dustiest cities in the world and the second-highest PM_{10} was reported from the city (5338 $\mu g/m^3$) in June 2010 across the Middle East area [16]. Based on World Health Organization (WHO) reports, Ahvaz is the fifth most polluted city in the world, with a mean annual PM_{10} of 231 $\mu g/m^{-3}$ and a mean annual $PM_{2.5}$ of 95 $\mu g/m^3$ in 2016 [17].

The occurrence of dust storms has increased enormously in the last two decades in west and SW Iran [6], and some studies have shown that the decreasing water level of the Tigris and Euphrates rivers in Iraq has led to the drying of the soil in that country, which accordingly, has led to the formation of new dust sources in the region [18–22]. The change in surface conditions in SW Iran is one of the most important factors in the increased activations of internal dust sources in this area [23]. The development of the horizontal pressure gradient between two systems of cyclone and anti-cyclone is one of the formation mechanisms of dust storms, as it increases the wind speed and leads to the development of low-level winds [24]. If the wind speed exceeds a threshold value above areas with dry soil, appropriate soil texture, and low vegetation, the dust particles start lifting into the atmosphere [25]. One of the mechanisms that results in an increase in the surface wind speed is the transfer of the momentum of the LLJ to the Earth's surface [26–28]. These jets have a core speed of more than 12 m/s between 975 and 875 hPa, along with the negative and positive wind shear at the top and bottom of the LLJ core, respectively [29–31]. The characteristics of LLJs and their formation time play an effective role in the severity and weakness of the dust storm phenomenon. Low-level jets, along with a maximum night speed in response to a night surface inversion, are common weather features in very arid and semi-arid regions [26].

There are different methods to investigate dust rising, transportation, and dispersion. It includes investigation of (i) surface measured reported data, (ii) satellite remote sensing data and images, (iii) dust modeling, (iv) forward and backward trajectory analysis, and (v) synoptic analysis [32–34]. Methods were used in the dust studies in the Middle East region to investigate dust storm generation and transportation [35–39]. In some cases, soil properties and vegetation cover were investigated during the dust, along with meteorological parameters such as wind speed, wind direction, precipitation, air temperature, and so on [21,40–42]. The studies showed a long drought in this area [6] along with a decrease in the water level of the rivers, especially the Tigris and Euphrates rivers in Iraq. This factor had an important role in growing the frequency of dust storms in the Middle East region [43–45]. Also, dust storms are mainly categorized into two main groups: Shamal dust storms and frontal dust storms [35,39,46–48], though haboob dust storms happen minimally in this region, too [49].

Although many studies investigated dust storms in SW Iran, and most of them focused on the dust particles raised from the deserts in Iraq, Syria, Saudi Arabia, and the southern coast of the Persian Gulf, only a few researchers have focused on dust rise from internal dust sources in SW Iran, and its causes and effects. In this study, two severe dust storms were investigated in southwest Iran. In both cases, dust particles were raised from the sources in SW Iran, and most of the stations in this area reported dust rising from around the stations. For this purpose, the outputs of the HYSPLIT and WRF-Chem models, along with satellite images, are analyzed in two dust cases. Furthermore, this research emphasizes the important and effective roles of LLJs in transferring momentum to the surface and strengthening surface winds.

2. Data Description and Methodology

2.1. Study Area

The study area is the Khuzestan province in the southwest of Iran, comprising 67,282 km^2. The area is located from 47°42′ E to 50°39′ E longitude and 29°58′ N to 32°58′ N (Figure 1). The northern to eastern parts are surrounded by mountains; the Zagros Mountain covers more than two-fifths of the area (approximately 300 km^2).

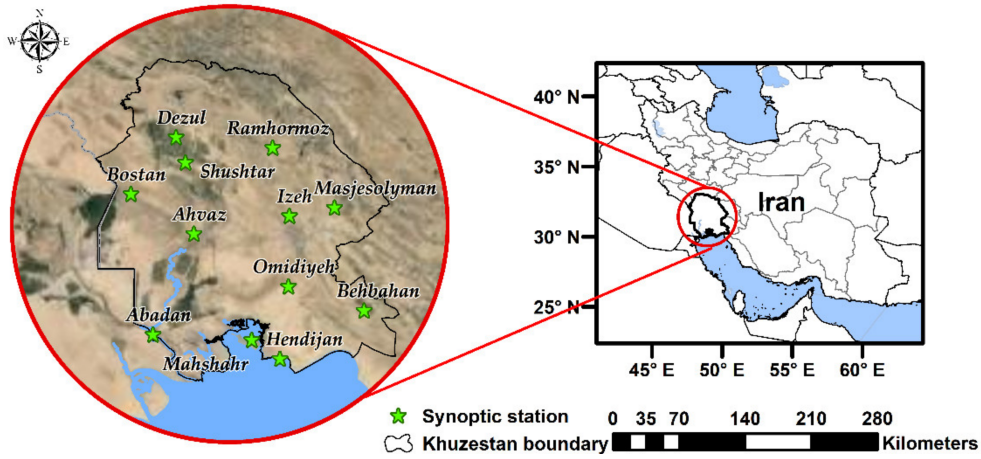


Figure 1. Study area with the synoptic weather stations in SW Iran. The green stars illustrate the synoptic stations.

Ahvaz (48°68′ E, 31°32′ N; 18 m) is one of the dustiest cities in the world located in this area [50]. Based on the World Health Organization (WHO), Ahvaz ranked as the most polluted city in the world in 2011 [23,50–53]. The city's air temperature rises to 50 degrees in summer, and the city is very hot and humid [51]. The city suffers from dust storms all around the year, especially during last spring and the summer [6]. According to the latest census, the population living in the area is more than 4.5 million people, and 72% of them live in the city and 28% live in the countryside. The occurrence of dust affects the health and livelihood of the population there.

In this study, the synoptic stations were selected to be considered in more detail. The location, longitude, latitude, and elevation are illustrated in Figure 1 and Table 1.

Table 1. The synoptic stations in southwest Iran.

Synoptic Station	Longitude	Latitude	Elevation (m)
Abadan	48.21° E	30.37° N	6
Ahvaz	48.60° E	31.33° N	22.5
Behbahan	50.22° E	30.60° N	313
Bostan	48.00° E	31.71° N	8.6
Dezful	48.43° E	32.25° N	82
Hendijan	49.70° E	30.24° N	3
Izeh	49.51° E	31.50° N	827
Mahshahr	49.15° E	30.54° N	6.2
Masjedsolyman	49.94° E	31.58° N	320.5
Omidiyeh	49.50° E	30.83° N	26
Ramhormoz	49.59° E	31.27° N	150
Shushtar	48.83° E	32.05° N	67

Khuzestan Province is affected by cross-border dust due to its proximity to the desert areas of Iraq, Syria, and Saudi Arabia. In addition, the internal conditions are suitable for the formation of local dust. During a 2014 study, the Iranian Mineral Exploration Unit of the Industry and Mining Organization identified and introduced the seven main hotspots that were active as dust sources in Khuzestan province (Figure 2). The result shows south Horul-Azim (Area 1) with 50,000 ha, north of Khorramshahr (Area 2) with 28,154 ha, east of Ahvaz (Area 3) with 15,620 ha, south and southeast of Ahvaz (Area 4) with 112,385 ha, Bandar Imam Khomeini to Omidiyeh (Area 5) with 86,147 ha, Mahshahr to Hendijan (Area 6) with 31,980 ha, east of Hendijan (Area 7) with 18,136 ha are the hotspots for local dust events [52–56].

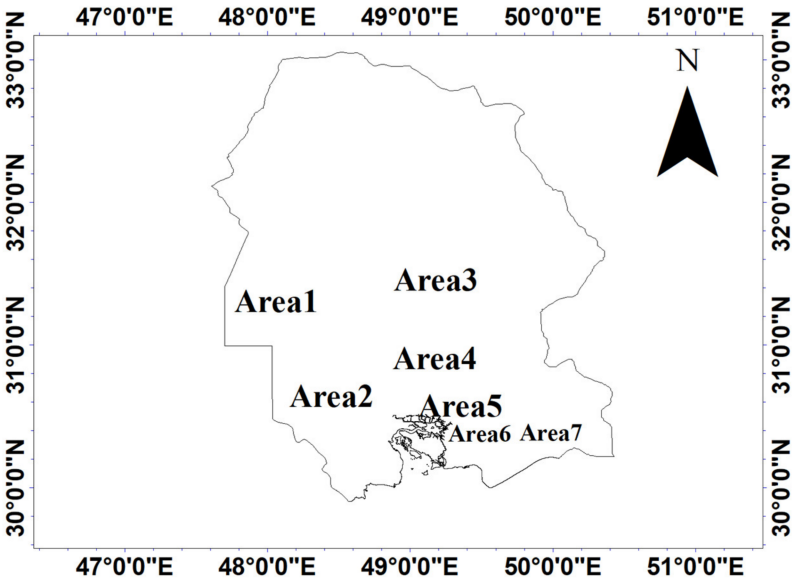


Figure 2. The seven hotspots of internal dust in Khuzestan province in SW Iran [52,56]. Horul-Azim, located in Area 1, north of Khorramshahr (Area 2), east of Ahvaz (Area 3), southeast of Ahvaz (Area 4), Bandar Imam Khomeini to Omidiyeh (Area 5), Mahshahr to Hendijan (Area 6), and east of Hendijan (Area 7).

2.2. Data

The meteorological data, including the present weather code, visibility, and 10-m winds, were provided by the Iranian Meteorology Organization (IRMO) at the selected station (Figure 1) from 2000 to 2020. The synoptic data is reported in 3-h intervals. The weather conditions are reported eight times per day. The present weather codes, 06, 07, 30 to 35, and 98, indicate dust with different mechanisms. The 07 code represents sand or dust raised by the wind near the synoptic station; thus, it is mostly related to local dust events [53–55].

In the next step, to study the dominant synoptic patterns and LLJ's mechanisms associated with the selected dust event, 6-h meteorological data, including mean sea level pressure, geopotential height at 500 hPa, wind field at 925 hPa, and 300 hPa, and divergence at 925 hPa and 300 hPa are analyzed using the ERA5 data [54]. The ERA5 data have a $0.25^0 \times 0.25^0$ spatial resolution with the hourly temporal resolution, available from 1000 hPa to 1 hPa (37 vertical levels) from 1940 to the present. This data was selected because of the fine spatial and temporal resolution.

2.3. Method

A visibility of less than 10,000 m associated with the present weather codes are the two criteria for calculating the dusty day number. The two severe local dust events on 29 January and 10 February 2015, were chosen for further consideration regarding the role of LLJs in activating local dust in Khuzestan Province. These events had the lowest horizontal visibility, with the 07 code being considered the local dust code [53]. The dust event criteria were severe local dust and take place in winter, when dust formation is not expected due to cold air and more precipitation. The least dusty days in Khuzestan occur in December and January, as mentioned by [55].

To understand the dust mechanism in the cold season for the two selected dust events, the synoptic–dynamic feature was analyzed using ERA5 data that was previously explained. Furthermore, the wind profile was plotted at 00:00, 03:00, 06:00, 09:00, and 12:00 UTC to investigate LLJ's role in local dust. The LLJ criteria, including the maximum wind speed value, the level of maximum wind speed (LLJ depth), and negative wind shear (LLJ strength), are mentioned in [56].

The backward trajectory of the particle was found by using the HYSPLIT model [57,58]. The backward trajectory can help to recognize dust sources and differentiate between local and cross-border dust. For this purpose, the Global Data Assimilation System (GDAS) with a horizontal resolution of 0.5 × 0.5 degree (GDAS0P5) was used to run the online HYSPLIT model with a backward time of 4 h at a 100-m height because the elevation is not the same in throughout the Khuzestan plain. For example, Ahvaz and Omidiyeh, with 22 and 26 m above mean sea level, is located in the center and southern parts of the Khuzestan plain, and also, local dust sources have around the same elevation exactly.

The backward trajectory calculated in the 3-h total run time ended at 06:00, 09:00, and 12:00 UTC, on 29 January and 10 February 2015.

In order to confirm and highlight the emission of dust mass, the MODIS true color image was used. The Aqua satellite, launched on 4 May 2002, is orbiting around the Earth with different instruments. The MODIS instruments have been operating since 2002 onboard the NASA Aqua satellites [59]. The Aqua satellite passes one time over a location in the day, so there is one image at a specific time for every day.

The concentration of surface dust and turbulence kinetic energy (TKE) are simulated by the implementation of the chemical numerical model WRF-Chem [60], version 3.9, in 27 km using GFS data for initial and boundary conditions with a resolution of 0.5 degrees. The model was configured to have a simulation domain (20–45° N, 30–60° E) using a horizontal resolution of 27 km and 32 vertical sigma levels (from 1000 hPa up to 10 hPa) in Figure 3.

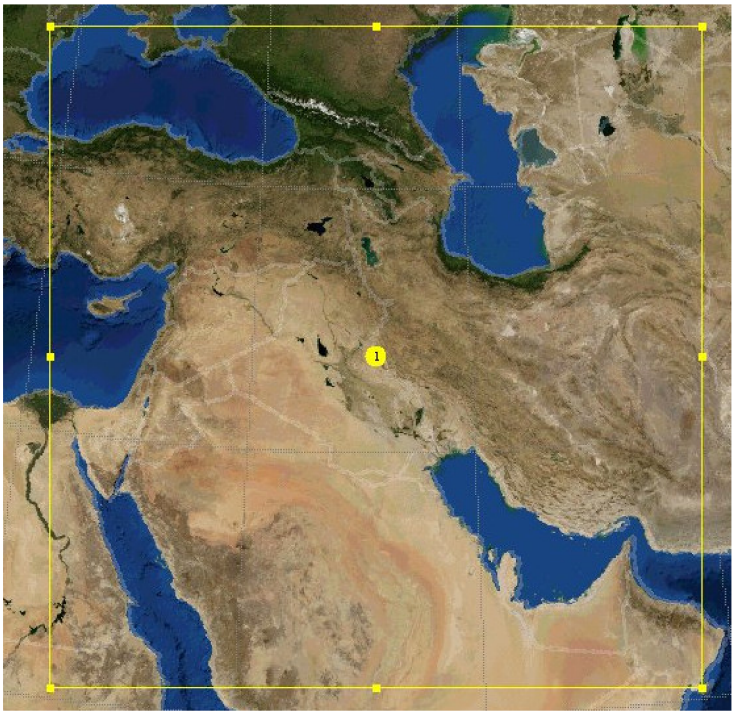


Figure 3. The WRF-Chem domain is shown by the yellow color line. The yellow central circul presents the first domain.

Table 2 shows the detailed WRF-Chem model configuration used for this study. For the dust scheme in the WRF-Chem model, the Air Force Weather Agency (AFWA) dust scheme was used [61].

The WRF-Chem model was run for two dust events from 00:00 UTC on 28 January 2015 to 00:00 UTC on 30 January 2015, and 00:00 UTC on 8 February 2015 to 00:00 UTC on 10 February 2015, the first 12 h of which were considered as the spin-up.

Table 2. WRF-Chem model settings used in this study.

Model Properties	Scheme
Resolution	27 km
Vertical level	32 level
Physics	
Cumulus	Grell 3D scheme [62]
PBL	Yonsei university scheme (YSU) [63]
Surface Layer	Monin-Obukhov (Janjic Eta) scheme [64]
Microphysics	WRF Single-Moment 5-class scheme [60]
Longwave Radiation	RRTM (rapid radiative transfer model) scheme [65]
Shortwave Radiation	Goddard shortwave [66]
Land surface process	Noah land surface model [67]
Chemical	
Chem_Opt = 401	4 bin Dust
emissions scenario Dust Scheme	AFWA [61,68]

The horizontal and vertical distribution of dust concentration, as well as the TKE vertical distribution simulated by WRF-Chem model output. The total dust concentration was calculated by adding up the concentrations from four dust particle sizes.

3. Results and Discussion

The dust mass has affected all selected stations from 2010 to 2020 in Khuzestan province (Table 3). Bostan, Abadan, and Dezful reported the highest mean annual dusty days, with 93.12, 88.4, and 82.7 days in a year, respectively.

Table 3. The mean annual number of dusty days in the selection station from 2010 to 2020.

Synoptic Station	Bostan	Abadan	Dezful	Masjedsolyman	Omidiyeh	Mahshahr	Ahvaz	Ramhormoz	Izeh	Behbahan	Shushtar	Hendijan
Mean annual of dusty days		88.4	82.7	74.8	66.6	62.9	64	52	50	49	44.6	43.8

Bostan experiences the dustiest days in Khuzestan Province, which is mentioned in a previous study [69]. The reason for that is the drying up of the Hur Al-Azim wetland and the construction of oil industries in the region, which act as dust sources. The same is represented in Figure 2. The cross-border dust mass increases dusty days in Abadan; also, local dust can increase the number of dusty days, as pointed out in [52], the second hotspot for local dust emission [52]. Omidiyeh and Mahshahr, located in the southern part of the area, are the two other dusty days' places in Khuzestan province. As a result, the higher dusty days occur in the south to the northwest of Khuzestan because of the influence of both cross-border and local dust.

Due to the highlands in the northeast of Khuzestan Province, these areas experience fewer dust phenomena, although the trapping of dust mass on the mountain slope is a factor in increasing the dust intensity. Ahvaz had 64 mean annual dust days, which is less than other cities, the dust intensity was higher, as mentioned in [16,17].

3.1. Vibility Reduction and 10-m Wind Speed

The mean daily visibility in synoptic stations on 29 January and 10 February 2015 is demonstrated in Figure 4a,b. The visibility reduction and the dust intensity are not the same at all stations. Also, maximum visibility reduction occurs at different daily times in both dust cases. The Behbahan, Omidiyeh, and Masjedsolyman located in eastern Khuzestan, had no visibility decrease because of dust on 29 January (Figure 4a). The city of Ahvaz experienced the lowest mean daily visibility on 29 January, with the highest dust intensity. The visibility reduction was recorded in the south and west parts of Khuzestan.

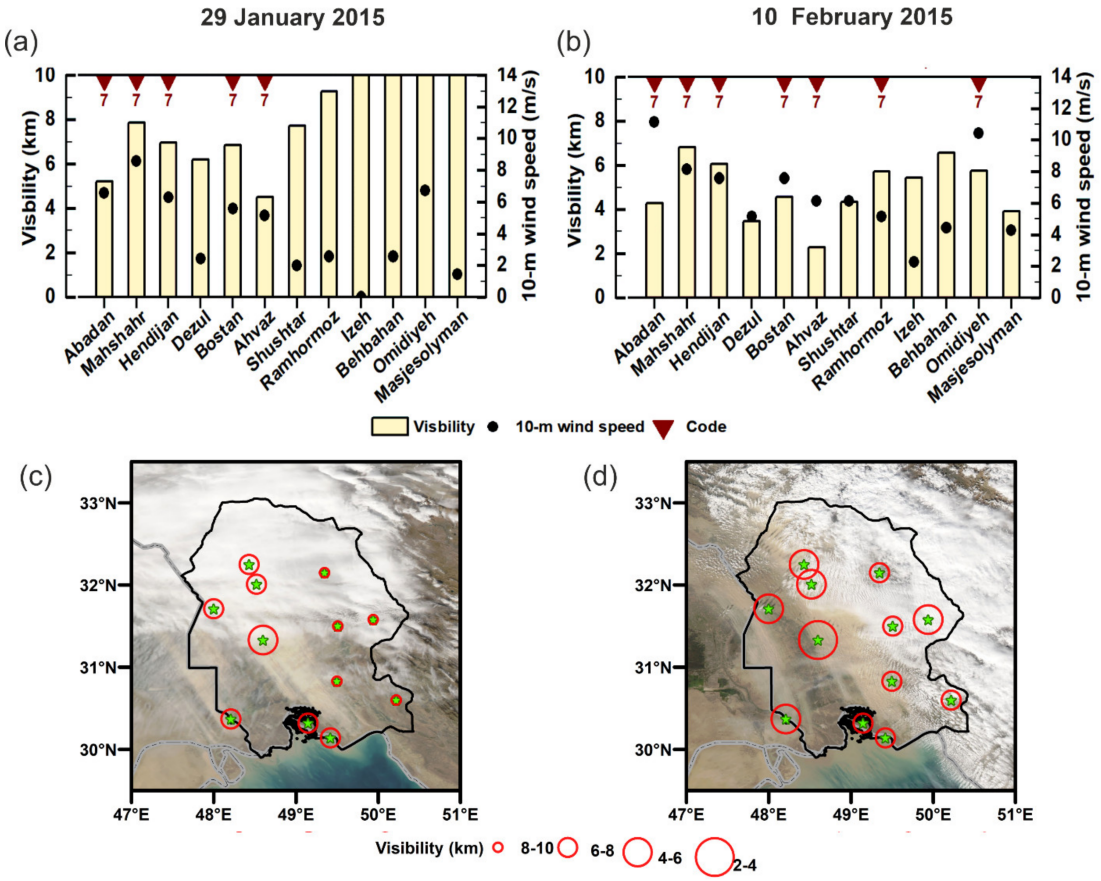


Figure 4. (**a**) The mean daily visibility (km) and 10-m wind speed (m/s) at the synoptic stations on 29 January 2015; (**b**) same as (**a**) on 10 February 2015. The red triangles indicate the present weather code. The local dust reported by 07 code. The MODIS true color image (**c**) at 09:29 UTC on 29 January 2015; (**d**) same as (**c**) at 09:52 UTC on 10 February 2015. The red open circle shows the visibility (km). The green stars represent the station location.

More stations experienced reduced visibility on 10 February due to dust (Figure 4b). The highest visibility reduction was found in Ahvaz on 10 February 2015 (Figure 4b). By comparing decreased horizontal visibility, it can be observed that the intensity and spread of dust were higher on 10 February rather than 29 January (Figure 4a,b). The important point is that the greatest reduction in horizontal visibility occurs in Ahvaz in two selected dust events.

The dust event was more intense in the southern parts of Khuzestan on 29 January, while it affected the northern parts the most on 10 February. Although the maximum daily of 10-m wind speed (6.2 m/s) was in Mahshar on 29 January (Figure 4c,d), it was not associated with the greatest decrease in visibility (Figure 4a). A greater increase of 10-m wind speed and a greater decrease in visibility were recorded on 10 February compared to 29 January (Figure 4a,b), which confirmed the role of 10-m wind speed in dust events.

The MODIS true color image at 09:29 UTC on 29 January 2015 and at 09:52 UTC on 10 February 2015 is illustrated in Figure 4c,d. Although most of Khuzestan Province was covered by clouds, the dust mass appeared in the free-cloud parts in two cases. The cloud cover prevents its underlying dust mass. The dust mass extended in a similar way in two dust cases, from the southern parts near Omidiyeh, Hendijan, and Mahshar, toward the northwest near Dezful, which is in harmony with the most visibility reduction in these stations (Figure 4a,b). The MODIS image showed widespread dust on 10 February 2015 (Figure 4d). There was less cloud cover and more dust extension on 10 February, which coincided with the horizontal visibility variation (Figure 4b).

The mean daily visibility is demonstrated in Figure 4c,d. The distribution of the dust mass and visibility reports were in agreement with each other, showing the dust spread from the south to the northwest of Khuzestan Province (Figure 4c,d). The highest concentration of dust on 10 January was in the west, but dust was widespread in the west and east of the Khuzestan Province on 10 February. The dust mass over the north of the Persian Gulf shows the cross-border dust from neighboring countries. It will be explained more by the HYSPLT pathway and wind direction at 850 hPa in the following.

As the highest dust intensity was observed in the south to the west of Khuzestan Province, the five stations located in this area were selected to consider the relationship between 10-m wind speed and visibility (Table 4). Also, these stations are in proximity to dry land, which is more prone to wind erosion. 10-m wind speed increased from 00:00 UTC to 09:00 or 12:00 UTC and reached its maximum value at 12:00 UTC on 29 January. The maximum 10-m wind speed recorded was 7, 9, 10, 11, and 15 m/s in Ahvaz, Abadan, Bostan, Hendijan, and Mahshahr, respectively, at 09:00 or 12:00 UTC on 29 January 2015. The maximum increase in 10-m wind speed occured between 06:00 and 09:00 UTC, at around 3 m/s in Abadan and 8 m/s in Mahshahr. The sudden and intense increase in 10-m wind speed can indicate the LLJ is breaking. The greatest reduction in visibility with 100, 200, 300, 2000, and 4500 m was recorded in Ahvaz, Abadan, Hendijan, Bostan, and Mahshahr, respectively, at 09:00 or 12:00 UTC on 29 January 2019. Given that wind speed increases three to six hours before a significant visibility reduction, the role of LLJ breaking is obvious in the increase of wind speed and local dust emission.

Table 4. Horizontal visibility (m) and 10-m wind speed (m/s) in Abadan, Ahvaz, Bostan, Hendijan, and Mahshahr in Khuzestan at 00:00, 06:00, 12:00, and 18:00 UTC on 29 January 2015 and on 10 February 2015.

		29 January 2015		**10 February 2015**	
Station	**Time (UTC)**	**10-m Wind Speed (m/s)**	**Visibility (m)**	**10-m Wind Speed (m/s)**	**Visibility (m)**
Abadan	00:00	3	7000	5	10,000
	03:00	6	7000	4	8000
	06:00	5	6000	12	3000
	09:00	10	200	18	100
	12:00	13	300	19	800
Ahvaz	00:00	2	7000	1	5000
	03:00	5	6000	2	6000
	06:00	5	8000	8	200
	09:00	8	200	6	100
	12:00	7	100	10	100
Bostan	00:00	5	10,000	5	10,000
	03:00	5	10,000	5	8000
	06:00	5	7000	6	6000
	09:00	10	2000	11	3000
	12:00	9	2000	10	800
Hendijan	00:00	0	10,000	0	10,000
	03:00	6	10,000	8	10,000
	06:00	5	10,000	11	300
	09:00	11	500	13	100
	12:00	10	300	12	4000
Mahshahr	00:00	8	10,000	2	10,000
	03:00	7	10,000	5	10,000
	06:00	7	10,000	9	7000
	09:00	15	2500	17	1800
	12:00	11	4500	10	7000

The 10-m wind speed in Ahvaz had a 7 m/s value, while the highest visibility reduction to 100 m took place, so dry land around Ahvaz is active as a local dust source with a lower wind speed than other cities. Although the maximum wind speeds of 10, 11, 13, 17, and 19 m/s occurred in Ahvaz, Bostan, Hendijan, Mahshahr, and Abadan at 09:00 to 12:00 UTC on 10 February 2015, the significant increase in wind speed occurred between 03:00 to 06:00 UTC. This can be explained by the interaction of the nocturnal LLJ with a synoptic structure. The visibilty reached 100, 100, 100, 1800, and 3000 m in Abadan, Ahvaz, Hendijan, Mahshahr, and Bostan at 12:00 UTC on 10 February 2015. The decreased visibility is associated with the maximum 10-m wind speed (Table 4). Hence, the relationship between 10-m wind speed and local dust emissions is well confirmed in two dust events in Khuzestan. The maximum 10-wind speed at five stations is more than 7 m/s, which is defined as the wind speed threshold for wind erosion and dust emission. The lack of a sharp reduction in visibility in Mahshahr compared to other stations is due to its closure to the Persian Gulf and wind direction, which will be investigated further.

3.2. HYSPLIT Model Simulations

Figure 5 shows the HYSPLIT model's backward trajectory output with the Lagrangian approach and the GDAS input data to determine the air mass trajectory and path of particles to the Ahvaz. Ahvaz city, located in the center of Khuzestan province, was targeted because it is surrounded by dust sources, has the highest visibility reduction in two dust cases, and is one of the dustiest cities in the world [70–72]. For this purpose, the horizontal tracking of the movement of dust particles for 06:00, 09:00, and 12:00 UTC with a time step of 3 h was carried out.

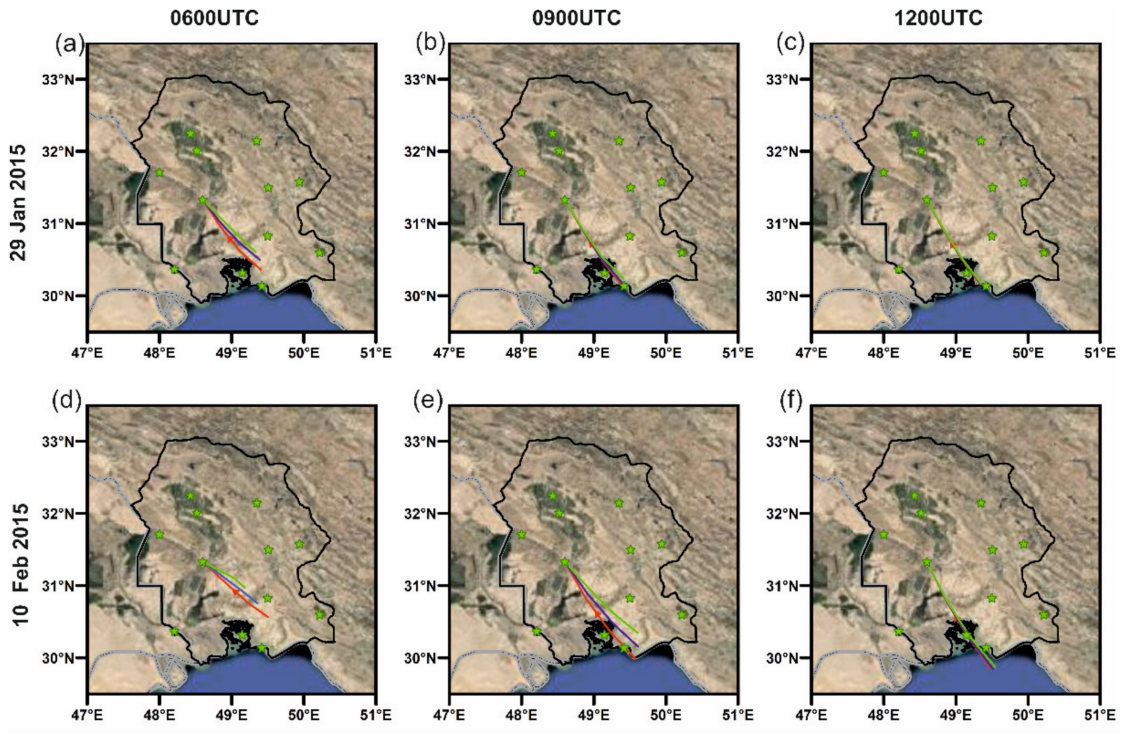


Figure 5. HYSPLIT output for a three hours backward trajectory in color lines at 100 m AGL ended at 06:00 (red), 09:00 (blue), and 12:00 (green) UTC, (**a**–**c**) on 29 January 2015, and (**d**–**f**) on 10 February 2015. The green stars represent the station location.

The particles pass from the southern and southeastern parts of the Khuzestan near Hendijan, Mahshar, and Omidiyeh toward Ahvaz in both cases (Figure 5). By comparing host spot dust sources (Figure 2) and the HYSPLIT backward path (Figure 5), it revealed the role of dry land as a local dust event on 29 January and 10 February 2015. The movement of dust particles can be seen in the southeast of Ahvaz, a dry land area, at 06:00 UTC on

10 February 2015 (Figure 5d–f), so the dust events had more intensity on 10 February rather than on 29 January. The HYSPLIT backward trajectory was according to the MODIS image (Figure 4c,d), which showed the dust mass spreading from south to north of Khuzestan.

3.3. Synoptic Investigation

The composition of the geopotential at 500 hPa and mean sea level pressure shows the formation of an active cyclone with a center of 1000 and 1004 hPa in the western part of the Mediterranean Sea at 00:00 and 06:00 UTC on 29 January 2015 (Figure 6). The low-pressure system with 1012 hPa was over north Saudi Arabia, Iraq, and SW Iran at 12:00 and 18:00 UTC on 29 January 2015. The southerly wind with increasing wind speed over Khuzestan province (Figure 5, third row) leads to the activation of local dust sources, and the dust emission is its consequence. The importance of southern winds in the lower layer of the atmosphere in the emission of local dust in Khuzestan province has been previously mentioned in some studies [55,73,74]. These winds play a significant role in carrying dust particles across the region, affecting visibility and air quality.

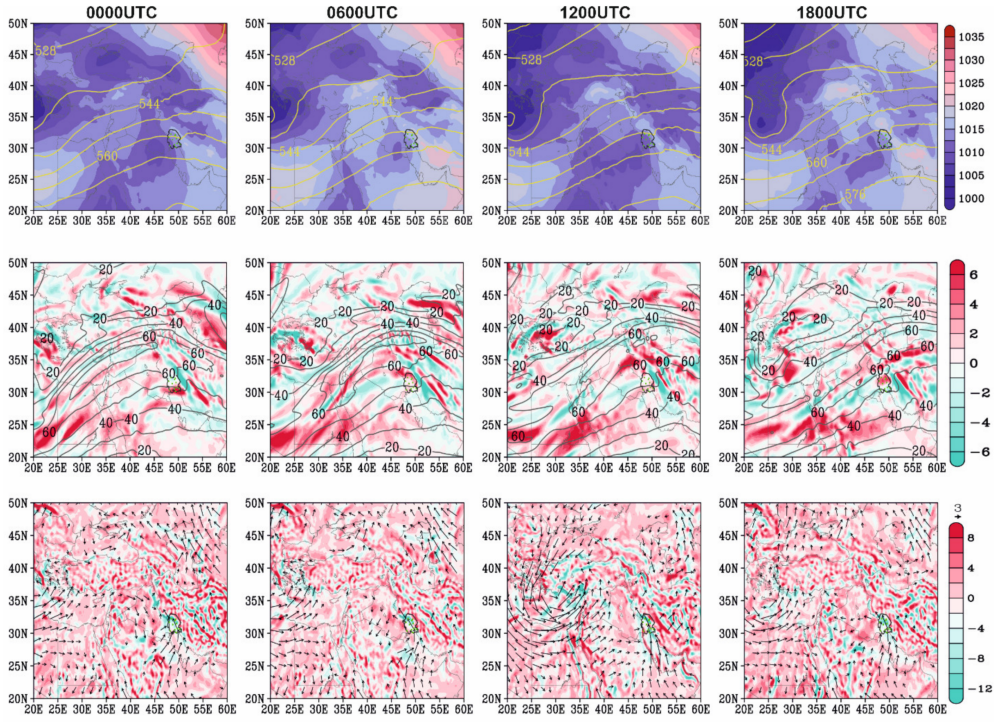


Figure 6. First row: mean sea level pressure in hPa (shaded), geopotential height at 500 hPa in gpm (yellow lines). Second row: wind speed in m/s (black lines) and divergence in $1/s \times 10^5$ (shaded) at 300 hPa. Third row: divergence in $1/s \times 10^5$ (shaded) and wind direction (black vector) at the 925 hPa level. The station's location is shown in the green circul, 00:00, 0:600, 12:00, and 18:00 UTC on 29 January 2015.

The decreasing visibility (Figure 4a) and MODIS image (Figure 4c) confirm the dust formation in Khuzesan. In addition, the backward path of the HYSPLIT model (Figure 5a–c) shows the airmass originated from a southerly wind direction, which demonstrates the role of wind speed and direction at lower levels of atmosphere in the dust emission and transportation.

On the other hand, the development and expansion of the high-pressure system over the Iranian plateau in the eastern part of the Khuzestan plain (with 1020 hPa) caused a strong pressure gradient and strengthened and developed the southerly winds over this area (Figure 6, first row). Examining the wind speed at 300 hPa shows the subtropical jet stream with a large cyclonic curve over Iran (Figure 6, second row). In the exit of the upper-level jet stream, a divergence zone can be seen at 00:00, 06:00, 12:00, and 18:00 UTC over the

Khuzestan plain in SW Iran (Figure 6, second row). The upper-level divergence associated with a cyclonic upper-level jet, collaboration on upward motion, and convergence at a lower level of the atmosphere is the consequence of decreasing mean sea level pressure and developing low pressure. Hence, the divergence at the level of 300 hPa leads to a convergence zone at 925 hPa (Figure 6, third row). The upward motion strengthened by convergence is the result of a dynamic weather system (not shown), which causes the lift-up of the dust particles to the middle atmosphere layer and its horizontal transfer to far away from sources. This is the reason why the dust mass spreads in the area (Figure 4c). Some of the selected stations in Khuzestan province are located on the left side of the wind speed core. So, the role of the LLJs in the formation of dust emissions may not be similar in all stations. This will be discussed in the next section.

The investigation of the mean sea level pressure associated with geopotential at 500 hPa indicates the development of low pressure with a central pressure of 996 hPa in the central part of the Mediterranean at 00:00 UTC on 10 February 2015 (Figure 7, first row). The low pressure strengthened due to decreasing pressure to 992 hPa as it moved eastward during 06:00 and 12:00 UTC. The easterly movement of toughe at 500 hPa into SW Iran caused the formation of a secondary low pressure center with 1008 hPa at 06:00 UTC in this area (Figure 7). Furthermore, the low-pressure system prevails until 18:00 UTC over the west of Iran. On the other hand, the expansion of the internal high-pressure system from the Iranian plateau towards the east of SW Iran and adjacent to the low-pressure system has strengthened the pressure gradient, and powerful southerly wind spreads over Khuzetan (first and third rows of Figure 7). The effect of strong southerly wind on the dust formation was explained above. The southerly wind spread from Saudi Arabia to southwest of Iran. Consequently, they can activate dust sources over Saudi Arabia [55]. As a result, Khuzestan province is affected by both cross-border and local dust sources, which can lead to an increase in dust concentration.

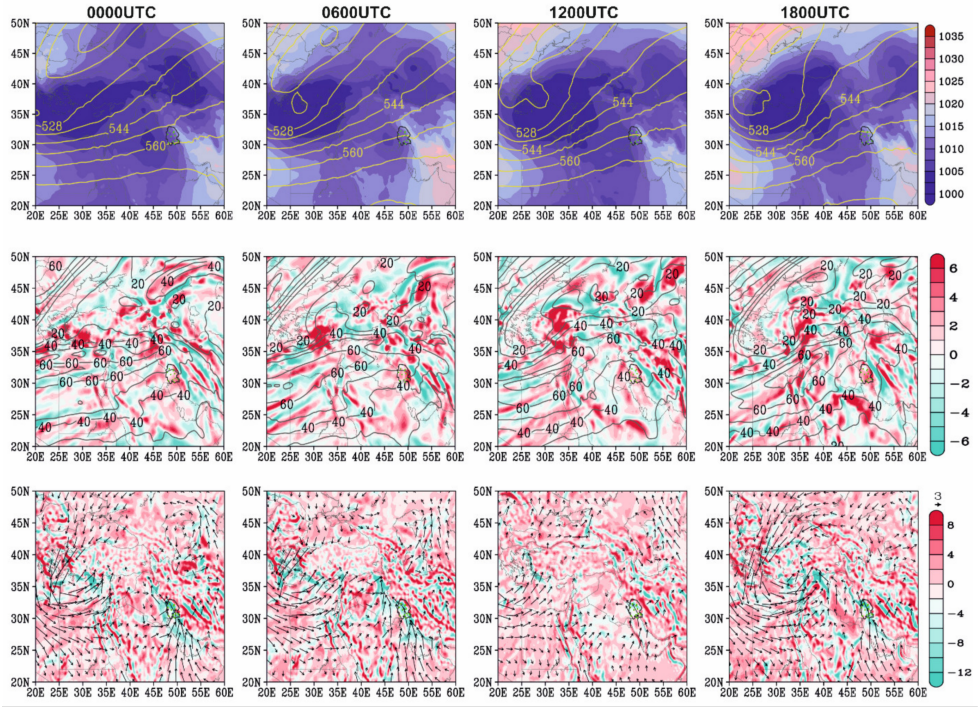


Figure 7. First row: mean sea level pressure in hPa (shaded), geopotential height at 500 hPa in gpm (yellow lines). Second row: wind speed in m/s (black lines) and divergence in $1/s \times 10^5$ (shaded) at 300 hPa and. Third row: divergence in $1/s \times 10^5$ (shaded) and wind direction (black vector) at the 925 hPa level. The station's location is shown in green circul, 00:00, 06:00, 12:00, and 18:00 UTC in 10 February 2015.

Examining the arrangement of the wind field at 300 hPa shows the role of the cyclonic curvature in subtropical jet stream exit to formation divergence over West Asia and Iran at 00:00, 06:00, and 12:00 UTC on 10 February (Figure 7, second row). The convergence in the column of air (Figure 7, third row) and upward motion (not shown) develops as the increasing the upper-level divergence (Figure 6, second row). The wind speed increased to 15 m/s over SW Iran at 925 hPa (Figure 7, third row), which will lead to an increase in the 10-m wind speed and dust emission. Its mechanism will be further discussed.

3.4. LLJ and Its Relationship with 10-m Wind Speed

The wind profile was used to represent the LLJ's formation in Abadan, Ahvaz, Mahshahr, Hendijan, and Bostan (Figure 8), where reported code 07 and experienced a decrease in visibility associated with increasing 10-m wind speed at 00:00, 06:00, and 12:00 UTC on 29 January and 10 February 2015. Also, stations are located on the left side of the wind speed core at 925 hPa (Figures 6 and 7, third row). The increase in wind speed between 975 to 950 hPa in Abadan, Ahvaz, and Bostan is more obvious on 29 January 2015 from 00:00 to 06:00 UTC (Figure 8, first row). The wind profile is similar in Abadan and Ahvaz, which are located on the left side of the LLJ (Figures 6 and 7, third row). Henijan and Mahshar, located in the eastern part had a similar wind profile too. The wind profile reveals that in the conditions of the formation of Genoese winds in Khuzestan province, the low-level jet is more pronounced on the left side of the jet axis and the wind speed is higher.

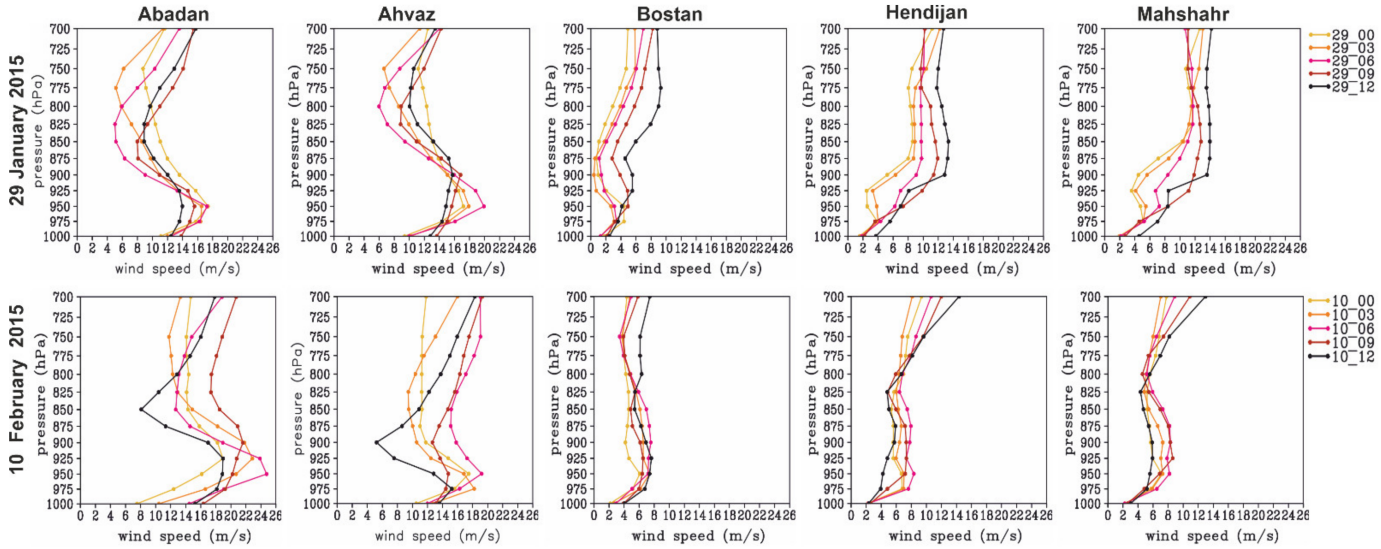


Figure 8. Wind profile of horizontal wind speed in (m/s), in Abadan, Ahvaz, Bostan, Hendijan, and Mahshahr in the Khuzestan province at 00:00, 03:00, 06:00, 09:00, and 12:00 UTC on 29 January (first row) and on 10 February (second row) 2015.

The maximum horizontal wind speed of 975-950 hPa in Ahvaz and Abadan, with 19.9 and 17.3 m/s, respectively, at 00:06 UTC on 29 January 2015 (Figure 8 and Table 5). The maximum wind speed at all stations is more than 12 m/s, which is the first criterion of the LLJ definition. The existence of a negative wind shear above (Table 5) at the maximum wind speed (LLJ core) confirms the second criterion of LLJ's identification. The greatest negative wind shear values of −13.9, and −12.2 m/s were obtained in Ahvaz and Abadan stations on 29 January 2015 (Table 5). The negative wind shear demonstrates LLJ's strength. As a result, the LLJ was strong in Ahvaz and Abadan, located in the western part of Khuzestan at 03:00 to 06:00 UTC on 29 January 2015.

Table 5. The LLJ criteria (maximum wind speed, positive and negative wind shear) in Ahvaz, Abadan, Mahshahr, Hendijan, and Bostan in Khuzestan at 00:00, 06:00, 12:00, 18:00 UTC on 29 January 2015 and on 10 February 2015.

		29 January 2015			10 February 2015		
Station	**Time (UTC)**	**Maximum Wind Speed Level**	**Wind Speed (m/s)**	**Wind Shear (-) (m/s)**	**Maximum Wind Speed Level (hPa)**	**Wind Speed (m/s)**	**Wind Shear (-) (m/s)**
Abadan	00	950	17.4	−8.6	950	17.5	−6.2
	03	950	16.5	−11.4	950	16.8	−8.7
	06	950	17.3	−12.2	950	19.2	−4.1
	09	950	15.6	−7.6	950	14.8	−2.1
	12	950	14	−5.1	975	15.2	−10.0
Ahavaz	00	950	17.2	−6	925	18.9	−4.8
	03	950	17.9	−11.3	925	22.9	−11.1
	06	950	19.9	−13.9	950	24.8	−12.1
	09	900	16.8	−8.0	900	21.6	−4.3
	12	900	15.8	−5.7	925	19.0	−10.9
Bostan	00	975	4.4	−3.7	950	6.1	−2.3
	03	975	3.1	−2.7	950	7.4	−3.7
	06	975	3.4	−2.3	900	7.5	−4.1
	09	950	4.9	−2.1	925	6.5	−2.6
	12	925	5.5	−1.0	925	7.6	−2.2
Hendijan	00	975	5.1	−1.5	975	6.8	−1.4
	03	950	5.5	−1.4	975	7.0	−1.0
	06	950	7.3	−0.5	950	8.3	−1.9
	09	850	12.8	−1.7	925	7.3	−2.5
	12				875	5.9	−1.1
Mahshahr	00	975	3.9	−1.4	950	7.1	−1.9
	03	975	4.0	−0.7	950	7.3	−2.4
	06	875	9.8	−0.2	950	8.2	−3.0
	09	875	11.9	−2.3	925	8.6	−4.0
	12	850	13.4	−1.5	925	5.9	−1.6

LLJ's broken or decreased wind speed in the LLJ core occured from 09:00 to 12:00 UTC (Figure 8), which causes the transfer of momentum or turbulence kinetic energy to the surface and increased 10-m wind speed. This is why the 10-m wind speed increased from 09:00 to 1200 m/s at 12:00 UTC in 29 January 2015 in the selected stations (Table 5). One of the mechanisms that leads to an increase in surface wind speed is known to be the transfer of momentum from the LLJ to the Earth's surface [26–28] (See Table 5). The increasing 10-m wind speed leads to local dust emissions. The visibility reduction to 100, 200, and 300 in Ahvaz, Abadan, and Hendijan, respectively, took place in Khuzestan province (Table 5).

The wind profile in Ahvaz and Abadan was similar, with increased wind speed at 975 to 950 hPa. In addition, the wind profile in Hendijan and Mahshahr was similar too. The wind speed at the vertical level in five selected stations had the same structure in the two dust events. The LLJ was stronger in February because of the greater wind speed and negative wind shear (Table 5), so that the maximum wind speed in the LLJ nose reached to 24.8 m/s and 19.2 m/s in Ahvaz and Abdan (Table 5). The LLJ depth in both dust cases did not differ. The stronger LLJ, associated with a stronger synoptic system, collaborated to increase dust intensity and spreation on 10 February.

3.5. WRF-Chem Dust Surface Concentration

The distribution of surface dust estimated by WRF-Chem, at 00:00, 06:00, 12:00, and 18:00 UTC on 29 January and 10 February 2015 are shown in Figure 9. The model simulated surface dust concentration increased more than 2000 $\mu g/m^3$ in SW Iran at 00:00 UTC on 29 January, and it is the development and spread of the dust mass over the northern parts of Khuzestan the next time. The surface dust distribution illustrates local dust activation. Also, dust concentration was not high over Kuwait, Saudi Arabia, and Iraq on 29 January 2015, which confirmed local dust in Khuzestan. Under normal circumstances, the dust storms

raised from Mesotopean plain and desert in Saudi Arabia affect Ahvaz and other cities in Southwest Iran [6]. However, in this case, dust particles were raised from the sources in Khuzestan dry land and affected the surrounding area.

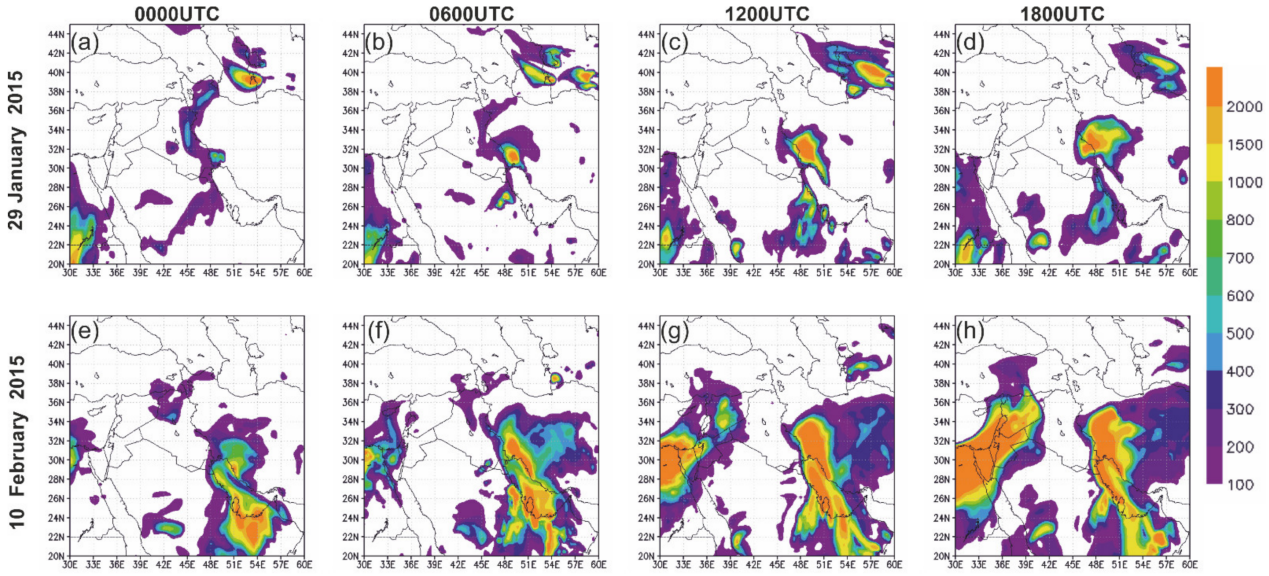


Figure 9. Simulation of the concentration of surface dust in μg/m^3 (shaded) by WRF-Chem model with a spatial resolution of 27 km at 00:00, 06:00, 12:00, 18:00 UTC (**a**–**d**) on 29 January (first row) and (**e**–**h**) 10 February (second row) 2015.

The WRF-Chem model simulated estimates of two high dust concentration centers over Kuwait, North Saudi Arabia, and SW Iran at 00:00 UTC on 10 February 2015 (Figure 9). The maximum dust concentration in Khuzestan province shows local dust activation. In comparison with the first case, dust particles rose from the larger area in the Middle East. This is due to the synoptic system and the spread of increasing southerly wind speed over the northern part of Saudi Arabia (Figure 7, third row). The dust surface was transported toward the Persian Gulf and central Iran the next time, which expressed the cooperation of the local and cross-border dust in increasing the dust in Khuzestan on 10 February.

By comparing the surface dust distribution of two dust events, it can be found that the synoptic system has led to the southerly winds and the LLJ formation, which resulted in the activation of local dust in Khuzestan province. Also, the spread of southerly wind speed caused cross-border dust, collaboration to increase dust intensity in the SW and central Iran. The surface dust transportation in the southerly direction coincides with the southerly wind, the HYSPLIT model, and MODIS image.

3.6. LLJ and Momentum in Dust Emission

The vertical cross-section of dust concentration and the amount of kinetic energy of WRF-Chem model are shown in Abadan, Ahvaz, Bostan, Hendijan, and Mahshahr (Figure 10). The LLJ formation and broken impact on transfer momentum from the LLJ core level to the surface and, consequently, the effects of this parameter on the 10-m wind speed associated with activation of dust sources on 29 January and 10 February 2015 is investigated by TKE.

The amount of TKE increases from 06:00 UTC to 12:00 UTC in all the stations, which leads to the transfer of momentum to the surface and the increase in the mixing in the lower layer of the atmosphere. The 10-m wind speed increased due to the transfer of momentum to the surface in this hour (Figure 10; first row and second row). The local dust emitted from the dry land surface in Khuzestan is based on broken LLJs, increasing upward momentum and wind speed. The dust particles rise to the higher layer due to increased mixing in the boundary layer. The dust mass reaches to the higher elevation in Ahvaz and Bostan on

29 January 2015. The TKE in Ahvaz was 1.8 m^2/s^2 around 06:00 UTC, which is associated with a higher level of dust transport. The vertical dust concentration is higher in Ahvaz, Bostan, and Mashahar. The dust particles lifted up to higher levels in Ahvaz, Mahshar, Bostan, and Hendijan on 10 February 2015. Therefore, dust vertical extension differs in all stations on 29 January and 10 February 2015, which depends on the synoptic system, wind file, and LLJ strength.

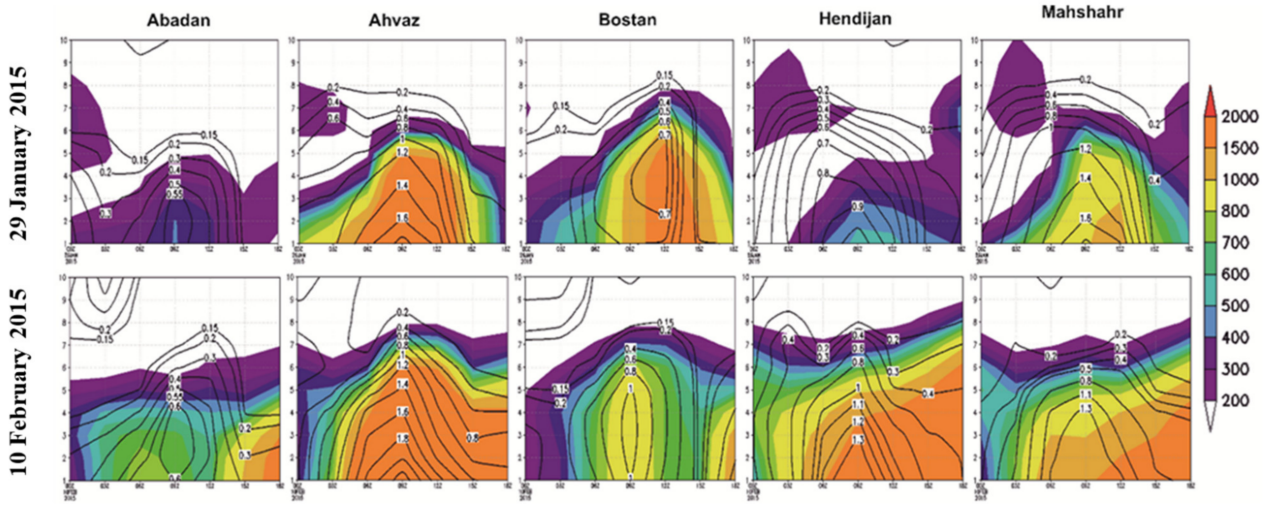


Figure 10. Vertical profile of dust concentration in $\mu g/m^3$ (shaded) and TKE in m^2/s^2 (black lines) WRF-Chem model at five meteorological stations of Abadan, Ahvaz, Bostan, Hendijan, and Mahshahr at 00:00, 03:00, 06:00, 09:00, 12:00, 15:00 and 18:00 UTC on 29 January (first row) and 10 February (second row) 2015.

The WRF-Chem output, including the TKE and dust vertical distribution, concluded in the LLJ breaking occurring at 09:00 UTC, about three hours before 12:00 UTC.

In the Abadan, Ahvaz, Handijan, and Bostan stations, the amount of kinetic energy in the second case was higher than in the first one. Due to the stronger jet in the 10 February dust, more kinetic energy is expected.

In Ahvaz and Abadan stations, the maximum spread of dust coincides with the maximum kinetic energy, which indicates the effect of jet failure and increase in kinetic energy in activating dust sources and increasing dust intensity. The maximum kinetic energy and maximum dust in Ahvaz, Abadan, and Bostan were obtained at 09:00 UTC, which confirms the previous analysis.

4. Conclusions

This study examined the two severe local dust storms in SW Iran through synoptic analysis, satellite images, HYSPLIT, and the WRF-Chem model. Khuzestan province is mostly affected by cross-border and rarely by internal dust sources. The two severe winter dust events with horizontal viability of less than 100 m in some stations in Khuzestan, formation from internal sources, were selected for study.

Investigating features such as the synoptic system, LLJ characteristic, horizontal dust distribution, vertical dust, and TKE were carried out on 10 February 2015 and 29 January 2015. Although the Khuzestan province is affected by dust mass, the dusty day numbers are different in meteorological stations. Bostan and Abadan have the dustiest day numbers due to their proximity to the eastern border of Iraq and the simultaneous impact of the local and cross-border dust.

The internal dust sources become active when the cyclonic curvature associated with upper-level divergence formed in the STJ exit over Khuzestan province. The minor trough collaborated to develop low pressure or pressure troughs along with southerly wind speed

in the winter season. The HYSPLIT backward trajectory shows the particles transfer from the south to the north of Khuzestan, which is in harmony with the southerly wind at 925 hPa.

The comparison of the characteristics of the LLJ, such as the intensity and weakness of the maximum speed, emphasizes the existence of a relationship between the low-level jet speed and the 10-m wind speed to local dust emission and decreased visibility in Khuzestan. The MODIS true color image confirmed the dust mass in this area.

The threshold of wind speed in the LLJ core to the rise of dust is different in the stations of Ahvaz, Abadan, Mahshahr, Omidiyeh, Hendijan, and Bostan on 29 January 2015 and 10 February 2015. The higher wind speed in the LLJ core and the negative wind shear led to more TKE, 10-m wind speed, and dust concentration on 10 February. Furthermore, the combined examination of the decrease in horizontal visibility, the increase of 10-m wind speed, and the amount of simulated TKE in both events of the dust phenomenon showed that the maximum concentration of dust particles along with the maximum momentum occurred at 09:00 UTC, which is the momentum transfer from the lower atmospheric jet to the surface and strengthening.

The near-surface wind speed increased when the LLJ is broken, and the momentum is transferred to the surface, resulting in dust emission. The WRF-Chem simulated this mechanism well in SW Iran. The WRF-Chem output showed acceptable dust concentration and confirmed activation of local dust in Khuzestan on 29 January and 10 February 2015. In addition, the dust surface concentration of the WRF-Chem model demonstrated the cross-border dust in Saudi Arabia collaborated with local dust and increased dust intensity in Khuzestan province.

Furthermore, the combined examination of the vertical dust concentration and the TKE simulated by the WRF-Chem show that the maximum dust concentration along with the maximum TKE occurred at 09:00 UTC, which emphasizes the increase in 10 m-wind speed in the next hours (12:00 UTC) due to the transfer of the momentum when the LLJ broke.

Author Contributions: Conceptualization, N.H.H. and R.P.; methodology, R.P., M.C.G.O. and E.M.H.; writing, review and software, N.H.H. and R.P.; validation, R.P., N.H.H., M.H. and A.-H.M.; formal analysis, N.H.H., R.P., A.-H.M. and M.H.; resources, A.-H.M., R.P. and M.C.G.O.; data curation, N.H.H.; writing—original draft preparation, R.P. and N.H.H.; writing—review and editing, M.C.G.O., R.P. and A.-H.M.; visualization, N.H.H., R.P., M.H. and E.M.H.; supervision, A.-H.M. All authors have read and agreed to the published version of the manuscript.

Funding: Open Access Funding by the University of Graz.

Institutional Review Board Statement: Not applicable.

Informed Consent Statement: Not applicable.

Data Availability Statement: Data sets supporting reported results are ERA-5 via https://www.ecmwf.int/en/forecasts/datasets/reanalysis-datasets/era5 (accessed on 1 December 2023).

Acknowledgments: The authors are greatly thankful to the ECMWF ERA-5 meteorological products that are used in the current work. We acknowledge the IRIMO (Iranian Meteorological Organization) for providing visibility and wind speed data for the two dust cases. The authors would also like to thank the University of Graz for providing funding for this research.

Conflicts of Interest: Nasim Hossein Hamzeh is an employee of the Air and Climate Technology Company (ACTC). The paper reflects the views of the scientists and not the company. The authors declare no conflict of interest.

References

1. Middleton, N. *Deserts: A Very Short Introduction*; Oxford University Press: Oxford, UK, 2009; Volume 215.
2. Al-Dousari, A. (Ed.) *Atlas of Fallen Dust in Kuwait*; Springer Nature: Berlin/Heidelberg, Germany, 2021.
3. Knippertz, P.; Stuut, J.B.W. *Mineral Dust—A Key Player in the Earth System*; Springer: Berlin/Heidelberg, Germany, 2014; pp. 121–147.

4. Khusfi, Z.E.; Khosroshahi, M.; Roustaei, F.; Mirakbari, M. Spatial and seasonal variations of sand-dust events and their relation to atmospheric conditions and vegetation cover in semi-arid regions of central Iran. *Geoderma* **2020**, *365*, 114225. [CrossRef]
5. Broomandi, P.; Dabir, B.; Bonakdarpour, B.; Rashidi, Y. Identification of dust storm origin in South–West of Iran. *J. Environ. Health Sci. Eng.* **2017**, *15*, 16. [CrossRef]
6. Hamzeh, N.H.; Kaskaoutis, D.G.; Rashki, A.; Mohammadpour, K. Long-term variability of dust events in southwestern Iran and its relationship with the drought. *Atmosphere* **2021**, *12*, 1350. [CrossRef]
7. Karegar, E.; Hossein Hamzeh, N.; Bodagh Jamali, J.; Ranjbar Saadat Abadi, A.; Moeinaddini, M.; Goshtasb, H. Numerical simulation of extreme dust storms in east of Iran by the WRF-Chem model. *Nat. Hazards* **2019**, *99*, 769–796. [CrossRef]
8. Hamidi, M.; Kavianpour, M.R.; Shao, Y. Numerical simulation of dust events in the Middle East. *Aeolian Res.* **2014**, *13*, 59–70. [CrossRef]
9. Karami, S.; Hamzeh, N.H.; Alam, K.; Noori, F.; Abadi, A.R.S. Spatio-temporal and synoptic changes in dust at the three islands in the Persian Gulf region. *J. Atmos. Sol.-Terr. Phys.* **2021**, *214*, 105539. [CrossRef]
10. Karami, S.; Hamzeh, N.H.; Kaskaoutis, D.G.; Rashki, A.; Alam, K.; Ranjbar, A. Numerical simulations of dust storms originated from dried lakes in central and southwest Asia: The case of Aral Sea and Sistan Basin. *Aeolian Res.* **2021**, *50*, 100679. [CrossRef]
11. Rashki, A.; Kaskaoutis, D.G.; Rautenbach, C.d.; Eriksson, P.G.; Qiang, M.; Gupta, P. Dust storms and their horizontal dust loading in the Sistan region, Iran. *Aeolian Res.* **2012**, *5*, 51–62. [CrossRef]
12. Rashki, A.; Kaskaoutis, D.G.; Francois, P.; Kosmopoulos, P.; Legrand, M. Dust-storm dynamics over Sistan region, Iran: Seasonality, transport characteristics and affected areas. *Aeolian Res.* **2015**, *16*, 35–48. [CrossRef]
13. MalAmiri, N.; Rashki, A.; Hosseinzadeh, S.R.; Kaskaoutis, D. Mineralogical, geochemical, and textural characteristics of soil and airborne samples during dust storms in Khuzestan, southwest Iran. *Chemosphere* **2022**, *286*, 131879. [CrossRef]
14. Ghasem, A.; Shamsipour, A.; Miri, M.; Safarrad, T. Synoptic and remote sensing analysis of dust events in southwestern Iran. *Nat. Hazards* **2012**, *64*, 1625–1638. [CrossRef]
15. Dargahian, F.; Lotfinasab Asl, S.; Khosroshahi, M.; Gohardoust, A. Determining the share of internal and external resources of dust in Khuzestan province. *Iran Nat.* **2017**, *2*, 36–41.
16. Shahsavani, A.; Naddafi, K.; Haghighifard, N.J.; Mesdaghinia, A.; Yunesian, M.; Nabizadeh, R.; Arahami, M.; Sowlat, M.; Yarahmadi, M.; Saki, H. The evaluation of PM_{10}, $PM_{2.5}$, and PM1 concentrations during the Middle Eastern Dust (MED) events in Ahvaz, Iran, from April through September 2010. *J. Arid Environ.* **2012**, *77*, 72–83. [CrossRef]
17. World Health Organization. Noncommunicable Diseases Country Profiles 2018. Available online: https://www.who.int/publications-detail-redirect/9789241514620 (accessed on 1 December 2023).
18. Middleton, N. Variability and trends in dust storm frequency on decadal timescales: Climatic drivers and human impacts. *Geosciences* **2019**, *9*, 261. [CrossRef]
19. Rashki, A.; Middleton, N.J.; Goudie, A.S. Dust storms in Iran–Distribution, causes, frequencies and impacts. *Aeolian Res.* **2021**, *48*, 100655. [CrossRef]
20. Hermida, L.; Merino, A.; Sánchez, J.; Fernández-González, S.; García-Ortega, E.; López, L. Characterization of synoptic patterns causing dust outbreaks that affect the Arabian Peninsula. *Atmos. Res.* **2018**, *199*, 29–39. [CrossRef]
21. Namdari, S.; Karimi, N.; Sorooshian, A.; Mohammadi, G.; Sehatkashani, S. Impacts of climate and synoptic fluctuations on dust storm activity over the Middle East. *Atmos. Environ.* **2018**, *173*, 265–276. [CrossRef] [PubMed]
22. Mohammadpour, K.; Sciortino, M.; Kaskaoutis, D.G. Classification of weather clusters over the Middle East associated with high atmospheric dust-AODs in West Iran. *Atmos. Res.* **2021**, *259*, 105682. [CrossRef]
23. Zarasvandi, A.; Carranza, E.; Moore, F.; Rastmanesh, F. Spatio-temporal occurrences and mineralogical–geochemical characteristics of airborne dusts in Khuzestan Province (southwestern Iran). *J. Geochem. Explor.* **2011**, *111*, 138–151. [CrossRef]
24. Barkan, J.; Alpert, P. Synoptic analysis of a rare event of Saharan dust reaching the Arctic region. *Weather* **2010**, *65*, 208–211. [CrossRef]
25. Westphal, D.L.; Toon, O.B.; Carlson, T.N. A case study of mobilization and transport of Saharan dust. *J. Atmos. Sci.* **1988**, *45*, 2145–2175. [CrossRef]
26. Washington, R.; Todd, M.C. Atmospheric controls on mineral dust emission from the Bodélé Depression, Chad: The role of the low level jet. *Geophys. Res. Lett.* **2005**, *32*. [CrossRef]
27. Knippertz, P. Dust emissions in the West African heat trough-the role of the diurnal cycle and of extratropical disturbances. *Meteorol. Z.* **2008**, *17*, 553. [CrossRef]
28. Schepanski, K.; Tegen, I.; Todd, M.; Heinold, B.; Bönisch, G.; Laurent, B.; Macke, A. Meteorological processes forcing Saharan dust emission inferred from MSG-SEVIRI observations of subdaily dust source activation and numerical models. *J. Geophys. Res. Atmos.* **2009**, *114*. [CrossRef]
29. Alizadeh Choobari, O.; Zawar-Reza, P.; Sturman, A. Low level jet intensification by mineral dust aerosols. *Proc. Ann. Geophys.* **2013**, *31*, 625–632. [CrossRef]
30. Fiedler, S.; Schepanski, K.; Heinold, B.; Knippertz, P.; Tegen, I. Climatology of nocturnal low-level jets over North Africa and implications for modeling mineral dust emission. *J. Geophys. Res. Atmos.* **2013**, *118*, 6100–6121. [CrossRef] [PubMed]
31. Heinold, B.; Knippertz, P.; Marsham, J.; Fiedler, S.; Dixon, N.; Schepanski, K.; Laurent, B.; Tegen, I. The role of deep convection and nocturnal low-level jets for dust emission in summertime West Africa: Estimates from convection-permitting simulations. *J. Geophys. Res. Atmos.* **2013**, *118*, 4385–4400. [CrossRef]

32. Salmabadi, H.; Khalidy, R.; Saeedi, M. Transport routes and potential source regions of the Middle Eastern dust over Ahvaz during 2005–2017. *Atmos. Res.* **2020**, *241*, 104947. [CrossRef]
33. Yu, Y.; Notaro, M.; Liu, Z.; Wang, F.; Alkolibi, F.; Fadda, E.; Bakhrjy, F. Climatic controls on the interannual to decadal variability in Saudi Arabian dust activity: Toward the development of a seasonal dust prediction model. *J. Geophys. Res. Atmos.* **2015**, *120*, 1739–1758. [CrossRef]
34. Mohammadpour, K.; Sciortino, M.; Saligheh, M.; Raziei, T.; Boloorani, A.D. Spatiotemporal regionalization of atmospheric dust based on multivariate analysis of MACC model over Iran. *Atmos. Res.* **2021**, *249*, 105322. [CrossRef]
35. Hamzeh, N.H.; Karami, S.; Kaskaoutis, D.G.; Tegen, I.; Moradi, M.; Opp, C. Atmospheric dynamics and numerical simulations of six frontal dust storms in the Middle East region. *Atmosphere* **2021**, *12*, 125. [CrossRef]
36. Abadi, A.R.S.; Hamzeh, N.H.; Shukurov, K.; Opp, C.; Dumka, U.C. Long-term investigation of aerosols in the Urmia Lake region in the Middle East by ground-based and satellite data in 2000–2021. *Remote Sens.* **2022**, *14*, 3827. [CrossRef]
37. Hamzeh, N.H.; Ranjbar Saadat Abadi, A.; Ooi, M.C.G.; Habibi, M.; Schöner, W. Analyses of a Lake Dust Source in the Middle East through Models Performance. *Remote Sens.* **2022**, *14*, 2145. [CrossRef]
38. Karami, S.; Hamzeh, N.H.; Alam, K.; Ranjbar, A. The study of a rare frontal dust storm with snow and rain fall: Model results and ground measurements. *J. Atmos. Sol.-Terr. Phys.* **2020**, *197*, 105149. [CrossRef]
39. Abadi, A.R.S.; Hamzeh, N.H.; Chel Gee Ooi, M.; Kong, S.S.-K.; Opp, C. Investigation of Two Severe Shamal Dust Storms and the Highest Dust Frequencies in the South and Southwest of Iran. *Atmosphere* **2022**, *13*, 1990. [CrossRef]
40. Gherboudj, I.; Beegum, S.N.; Ghedira, H. Identifying natural dust source regions over the Middle-East and North-Africa: Estimation of dust emission potential. *Earth-Sci. Rev.* **2017**, *165*, 342–355. [CrossRef]
41. Rezazadeh, M.; Irannejad, P.; Shao, Y. Climatology of the Middle East dust events. *Aeolian Res.* **2013**, *10*, 103–109. [CrossRef]
42. Moridnejad, A.; Karimi, N.; Ariya, P.A. A new inventory for middle east dust source points. *Environ. Monit. Assess.* **2015**, *187*, 582. [CrossRef] [PubMed]
43. Barlow, M.; Zaitchik, B.; Paz, S.; Black, E.; Evans, J.; Hoell, A. A review of drought in the Middle East and southwest Asia. *J. Clim.* **2016**, *29*, 8547–8574. [CrossRef]
44. Al Ameri, I.D.; Briant, R.M.; Engels, S. Drought severity and increased dust storm frequency in the Middle East: A case study from the Tigris–Euphrates alluvial plain, central Iraq. *Weather* **2019**, *74*, 416–426. [CrossRef]
45. Zoljoodi, M.; Didevarasl, A.; Saadatabadi, A.R. Dust events in the western parts of Iran and the relationship with drought expansion over the dust-source areas in Iraq and Syria. *Atmos. Clim. Sci.* **2013**, *3*, 321–336. [CrossRef]
46. Yu, Y.; Notaro, M.; Kalashnikova, O.V.; Garay, M.J. Climatology of summer Shamal wind in the Middle East. *J. Geophys. Res. Atmos.* **2016**, *121*, 289–305. [CrossRef]
47. Karami, S.; Kaskaoutis, D.G.; Kashani, S.S.; Rahnama, M.; Rashki, A. Evaluation of nine operational models in forecasting different types of synoptic dust events in the Middle East. *Geosciences* **2021**, *11*, 458. [CrossRef]
48. Karami, S.; Hamzeh, N.H.; Abadi, A.R.S.; Madhavan, B.L. Investigation of a severe frontal dust storm over the Persian Gulf in February 2020 by CAMS model. *Arab. J. Geosci.* **2021**, *14*, 2041. [CrossRef]
49. Miller, S.D.; Kuciauskas, A.P.; Liu, M.; Ji, Q.; Reid, J.S.; Breed, D.W.; Walker, A.L.; Mandoos, A.A. Haboob dust storms of the southern Arabian Peninsula. *J. Geophys. Res. Atmos.* **2008**, *113*. [CrossRef]
50. Shahsavani, A.; Naddafi, K.; Jaafarzadeh Haghighifard, N.; Mesdaghinia, A.; Yunesian, M.; Nabizadeh, R.; Arhami, M.; Yarahmadi, M.; Sowlat, M.H.; Ghani, M. Characterization of ionic composition of TSP and PM 10 during the Middle Eastern Dust (MED) storms in Ahvaz, Iran. *Environ. Monit. Assess.* **2012**, *184*, 6683–6692. [CrossRef] [PubMed]
51. Broomandi, P.; Dabir, B.; Bonakdarpour, B.; Rashidi, Y. Mineralogical and chemical characterization of suspended atmospheric particles in Ahvaz. *Int. J. Environ. Res.* **2017**, *11*, 55–62. [CrossRef]
52. Hejazi, S.J. Transferring flood to the dust sources of the province of Khuzestan (Southwest Iran): A multipurpose approach to water resource management. *Arab. J. Geosci.* **2022**, *15*, 332. [CrossRef]
53. O'Loingsigh, T.; McTainsh, G.; Tews, E.; Strong, C.; Leys, J.; Shinkfield, P.; Tapper, N. The Dust Storm Index (DSI): A method for monitoring broadscale wind erosion using meteorological records. *Aeolian Res.* **2014**, *12*, 29–40. [CrossRef]
54. Berrisford, P.; Dee, D.; Poli, P.; Brugge, R.; Fielding, K.; Fuentes, M.; Kållberg, P.; Kobayashi, S.; Uppala, S.; Simmons, A. The ERA-Interim archive Version 2.0, Shinfield Park. *Reading* **2011**, *1*, 23.
55. Mobarak Hassan, E.; Alizadeh, O. Dust events in southwestern Iran: Estimation of PM10 concentration based on horizontal visibility during dust events. *Int. J. Climatol.* **2022**, *42*, 5159–5172. [CrossRef]
56. Liu, H.; He, M.; Wang, B.; Zhang, Q. Advances in low-level jet research and future prospects. *J. Meteorol. Res.* **2014**, *28*, 57–75. [CrossRef]
57. Draxler, R.R.; Hess, G. An overview of the HYSPLIT_4 modelling system for trajectories. *Aust. Meteorol. Mag.* **1998**, *47*, 295–308.
58. Stein, A.; Draxler, R.R.; Rolph, G.D.; Stunder, B.J.; Cohen, M.D.; Ngan, F. NOAA's HYSPLIT atmospheric transport and dispersion modeling system. *Bull. Am. Meteorol. Soc.* **2015**, *96*, 2059–2077. [CrossRef]
59. Bright, J.M.; Gueymard, C.A. Climate-specific and global validation of MODIS Aqua and Terra aerosol optical depth at 452 AERONET stations. *Sol. Energy* **2019**, *183*, 594–605. [CrossRef]
60. Hong, S.-Y.; Dudhia, J.; Chen, S.-H. A revised approach to ice microphysical processes for the bulk parameterization of clouds and precipitation. *Mon. Weather Rev.* **2004**, *132*, 103–120. [CrossRef]

61. Marticorena, B.; Bergametti, G. Modeling the atmospheric dust cycle: 1. Design of a soil-derived dust emission scheme. *J. Geophys. Res. Atmos.* **1995**, *100*, 16415–16430. [CrossRef]
62. Grell, G.A.; Dévényi, D. A generalized approach to parameterizing convection combining ensemble and data assimilation techniques. *Geophys. Res. Lett.* **2002**, *29*, 38-31–38-34. [CrossRef]
63. Hong, S.-Y.; Noh, Y.; Dudhia, J. A new vertical diffusion package with an explicit treatment of entrainment processes. *Mon. Weather Rev.* **2006**, *134*, 2318–2341. [CrossRef]
64. Chen, F.; Janjić, Z.; Mitchell, K. Impact of atmospheric surface-layer parameterizations in the new land-surface scheme of the NCEP mesoscale Eta model. *Bound.-Layer Meteorol.* **1997**, *85*, 391–421. [CrossRef]
65. Mlawer, E.J.; Taubman, S.J.; Brown, P.D.; Iacono, M.J.; Clough, S.A. Radiative transfer for inhomogeneous atmospheres: RRTM, a validated correlated-k model for the longwave. *J. Geophys. Res. Atmos.* **1997**, *102*, 16663–16682. [CrossRef]
66. Chou, M.-D.; Suarez, M.J. An Efficient Thermal Infrared Radiation Parameterization for Use in General Circulation Models. 1994. Available online: https://citeseerx.ist.psu.edu/document?repid=rep1&type=pdf&doi=89b5ba55c9c4527da0ddaeacce2891605d02cd43 (accessed on 28 November 2023).
67. Niu, G.Y.; Yang, Z.L.; Mitchell, K.E.; Chen, F.; Ek, M.B.; Barlage, M.; Kumar, A.; Manning, K.; Niyogi, D.; Rosero, E. The community Noah land surface model with multiparameterization options (Noah-MP): 1. Model description and evaluation with local-scale measurements. *J. Geophys. Res. Atmos.* **2011**, *116*. [CrossRef]
68. LeGrand, S.L.; Polashenski, C.; Letcher, T.W.; Creighton, G.A.; Peckham, S.E.; Cetola, J.D. The AFWA dust emission scheme for the GOCART aerosol model in WRF-Chem v3. 8.1. *Geosci. Model Dev.* **2019**, *12*, 131–166. [CrossRef]
69. Abbasi, H.R.; Opp, C.; Groll, M.; Gohardoust, A.; Rouhipour, H. Wind regime and aeolian sand transport in Khuzestan Sand Sea. *Aeolian Res.* **2021**, *53*, 100746. [CrossRef]
70. Middleton, N. Dust storm hazards. *E3S Web Conf.* **2019**, *99*, 04001. [CrossRef]
71. Neisi, A.; Goudarzi, G.; Akbar Babaei, A.; Vosoughi, M.; Hashemzadeh, H.; Naimabadi, A.; Mohammadi, M.J.; Hashemzadeh, B. Study of heavy metal levels in indoor dust and their health risk assessment in children of Ahvaz city, Iran. *Toxin Rev.* **2016**, *35*, 16–23. [CrossRef]
72. Boloorani, A.D.; Shorabeh, S.N.; Samany, N.N.; Mousivand, A.; Kazemi, Y.; Jaafarzadeh, N.; Zahedi, A.; Rabiei, J. Vulnerability mapping and risk analysis of sand and dust storms in Ahvaz, IRAN. *Environ. Pollut.* **2021**, *279*, 116859. [CrossRef] [PubMed]
73. Daniali, M.; Karimi, N. Spatiotemporal analysis of dust patterns over Mesopotamia and their impact on Khuzestan province, Iran. *Nat. Hazards* **2019**, *97*, 259–281. [CrossRef]
74. Khalidy, R.; Salmabadi, H.; Saeedi, M. Numerical simulation of a severe dust storm over Ahvaz using the HYSPLIT model. *Int. J. Environ. Res.* **2019**, *13*, 161–174. [CrossRef]

Disclaimer/Publisher's Note: The statements, opinions and data contained in all publications are solely those of the individual author(s) and contributor(s) and not of MDPI and/or the editor(s). MDPI and/or the editor(s) disclaim responsibility for any injury to people or property resulting from any ideas, methods, instructions or products referred to in the content.